Mechanics of Advanced Composite Structures 10 (2023) 123 – 136

Semnan University

Mechanics of Advanced Composite Structures

journal homepage: http://MACS.journals.semnan.ac.ir

Flexural Behaviour of Nanocomposite Plate with CNT Distribution and Agglomeration Effect

M. C. Maurya [a*], S. M. Ali Jawaid [a], A. Chakrabarti [b]

[a] *Department of Civil Engineering, Madan Mohan Malaviya University of Technology, Gorakhpur-273010, India*
[b] *Department of Civil Engineering, Indian Institute of Technology, Roorkee-247667, India*

KEYWORDS

Nanocomposite plate;
Higher order shear deformation theory;
SWCNT;
Agglomeration;
FEM.

ABSTRACT

The behavior of various CNT distributions with agglomeration effects on FG plates is investigated in this paper under static loading. Here, to model the FG plate third-order shear deformation theory has been used and a FEM code has been developed. In the current higher-order shear deformation theory, transverse shear stresses are represented by quadratic variation along the thickness direction, resulting in no need for a shear correction factor. The properties of randomly oriented nano-inclusions are estimated using the two-parameter agglomeration model of Eshelby-Mori Tanaka. Next, the present approach is implemented with the FEM by employing a C^0 continuous isoparametric Lagrangian FE model with seven nodal unknowns per node. The static response of CNT reinforced composite plate with the influence of inclusions is explored by altering the agglomeration parameters and through-thickness CNT distribution pattern. The obtained results suggest that ignoring the agglomeration effect on CNT may result in erroneous results for various static responses. Since the author could not find any results in the static response of CNT-reinforced plates with the agglomeration effect, the proposed model is validated with the results corresponding to the isotropic plate. The impact of several agglomeration phases on the static behavior of a square plate is then studied parametrically.

1. Introduction

The carbon nanotubes were first discovered by Radushkevich et. al. in 1952 [1] and were used later by Iijima in 1991, which sparked a flurry of study into their possible industrial uses [2]. CNTs have been considered nano-scale reinforcement elements, which have shown promising results in improving a wide range of properties for engineering problems. Because of their exceptional strength, low density, and high Young's Modulus, CNTs are considered the ideal reinforcements of various composites. Outstanding thermal, mechanical, and electrical properties of CNT have been demonstrated in several types of research. These experiments thus created the concept of utilizing these inclusions as a reinforcement phase in some composite materials, to enhance their properties, especially mechanical ones. The term "nanocomposite structures" was coined as a consequence of this idea. To pinpoint the precise impact of CNTs on the mechanical behavior of nanocomposite structures, numerous techniques and approaches have been devised. A carbon nanotube-reinforced composite structure is investigated using the theory of mixtures, which is the approach that is most typically employed to study its overall properties. The theory of mixing provides a simple yet effective method for determining the mechanical properties of these nanostructures. In other words, this approach has been used in many papers dealing with various structural problems. The static response using the theory of mixture has been studied in [3], whereas other behaviors of CNT-reinforced composites have been investigated in [4].

It should be noted that the theory of mixture is quite limited because it does not consider several details that relate to the micromechanics of the nanoparticles. While the popular Mori-Tanaka method is based on assumption that

* Corresponding author. Tel.: +91-9451800047
E-mail address: mcmce@mmmut.ac.in

DOI: 10.22075/macs.2022.28078.1426
Received 2022-08-16; Received in revised form 2022-10-11; Accepted 2022-10-21.

there exist only two-phase (matrix and reinforcement), and they are perfectly bonded to each other. The Mori-Tanaka method has been used extensively in the literature to estimate the global properties of composites with great precision when the reinforcements are micrometer-scale or larger. Taking into account the occurrence of two phases appears to be reasonable at larger scales. It has been proven, however, that nanometer-sized reinforcement strongly perturbs the molecular structure of the polymer matrix at the reinforcement/polymer contact, and that this perturbed region has the same length scale as the nanometer-sized reinforcement. Therefore, a simple two-phase description of the reinforcement and neighboring polymer region fails at the nanoscale scale. Thus, the Mori–Tanaka model is not expected to perform well for nanostructured reinforcements [29]. In particular, CNTs are aggregated in particular areas of polymer composites used in strengthening, and this has been well captured and investigated by Shi et. al. [5], which obtained expressions that are analytical to calculate the Carbon nanotube's efficient mechanical properties, to take into consideration the agglomeration effect and the use of an equivalent continuum model founded on Eshelby-Mori-Tanaka approach [6]. This technique requires nanoparticles to represent their constitutive relationships according to the Hills elastic module. The micromechanical model that has recently been established is the beginning point for the current investigation to examine the static response in the agglomeration phase CNT-strengthened nanocomposite plate. Tornabene et. al. [7] proposed the use of the Generalized Differential Quadrature (GDQ) technique to analyze agglomerated CNT-reinforced nanocomposite plates and shells. The modification of agglomeration characteristics, as well as the through-the-thickness carbon nanotube pattern that reflects the CNT volume %, are investigated in the research to see how the reinforcing phase affects the flexural behavior of these plates reinforced by nanofillers. However, they used a hybrid plate model in this study. Ansari et. al. [17,18] studied the static and dynamic response of functionally graded carbon nanotube (FG-CNT)-reinforced rhombic laminates using a cubic variation of thickness coordinate in the displacement field in terms of Taylor's series expansion, which represents the higher-order transverse cross-sectional deformation modes. The final material properties of FG-CNT-reinforced rhombic laminates are estimated using the rule of mixture. The obtained numerical results were compared with the results available in the literature to verify the reliability of the present model. Finally, this study investigates the effect of CNT distribution, loading pattern, volume fraction, and various combinations of boundary constraints by developing a finite element code in FORTRAN. Md. Irfan Ansari and A. Kumar [19] studied the functionally graded carbon nanotube (CNT)-reinforced doubly curved singly ruled composite truncated cone. In this study, the developed mathematical model contains the expansion of Taylor's series up to the third degree of thickness coordinate and normal curvatures in in-plane displacement fields. In the developed model the condition of zero-transverse shear strain at the upper and lower surface of the truncated cone is applied. The advancement in the present mathematical model was the simultaneous inclusion of normal curvatures in the deformation field and twist curvature in strain-displacement equations. After validation, a large number of flexural problems were presented by varying different boundary conditions, volume fractions, loading patterns, and geometric parameters, and the developed results show good agreement with experimental results. Ansari and A. Kumar [20] investigated the bending behavior of functionally graded carbon nanotube (CNT) reinforced doubly curved singly ruled truncated rhombic cone. For the analysis, a simple C^0 isoparametric finite element formulation based on third-order shear deformation theory was used. Finally, the proposed model was validated with analytical, experimental, and finite element results from the literature with good agreement. R. Kumar and A. Kumar [21] did a free vibration analysis of multiscale functionally graded plates, reinforced with a carbon nanotube using modified third-order shear deformation theory with a variation in transverse displacement. In the analysis, a rectangular nine-noded element containing 117 nodal unknowns at each element was considered. The top and bottom transverse shear stresses of the plate were considered zero. The effective elastic properties of the multiscale composite plate are estimated by the combination of the Halpin–Tsai equation and the homogenization scheme. After that various parametric study was done. Zghal et. al. [22-24, 27-28] investigated the linear static, Free vibration, Nonlinear and large deflection based on the geometric nonlinearity behavior of functionally graded carbon nanotube-reinforced plates and shells. In the study five types of CNT distributions were considered, that is, uniform and four kinds of functionally graded distributions along the thickness of shell structures. The governing equations were developed based on a discrete double directors shell finite element. Finally, the overall structure behavior was studied with the effects of carbon nanotube volume fraction, length-to-thickness

ratio, boundary conditions, and other geometrical parameters. Frikha et. al [25-26] studied the dynamic behavior of functionally graded carbon nanotubes-reinforced plate and shell structures using a double directors finite shell element. The researchers also contributed to the field of functionally graded carbon nanotubes-reinforced thin composite shells using Finite rotation three and four nodes shell elements and, in the end, the predicted behavior of such structures was examined with good agreement.

It may be observed from the above literature review that very few works are based on a thorough examination of functionally graded plates with the inclusion of agglomerated carbon nanotubes by applying higher-order shear deformation theory. This paper has, therefore, tried to develop a FEM based on a theory of HSDT, including the impact of the parameter above. A C^0 finite element model with seven nodal unknowns per node is used to conduct the analysis. Various CNT distributions through the thickness of the plate such as UD (uniformly distributed CNT) and FG-V (unsymmetrically distributed CNT) through the plate thickness with the effect of agglomeration are considered in the present analysis. The FGM property, which covers Young's Modulus (E) and Poisson Ratios (v), is represented by Eshelby–Mori–Tanaka approach of the two-parameter model of agglomeration of nano-Inclusions that are randomly dispersed [5]. The effects of agglomeration parameters ξ & ζ with three different types of CNT's volume fraction distributions were considered in this research to get the static response of the simply supported square FG plate. Many parametric studies are conducted to generate new benchmark results.

2. Material Modelling

For any structural analysis, Material modeling is very important. The application of CNT-reinforced composite structures demands to development of detailed modeling of the effective material properties of a such composite at the macroscopic level. Because molecular dynamics or other atomistic models are computationally intensive, micromechanical methods are used to describe the behavior of these materials in this work. Material modeling of FG-CNTRC is presented using the Mori-Tanaka method considering the effect of agglomeration of CNT for various types of CNT distributions.

2.1. Material Modelling of FG-CNTRC

The FG-CNTRC material is considered to be made up of an isotropic matrix (e.g., epoxy resin) and fiber (CNTs), with material qualities graded along the direction of thickness of the plate as per linear distribution (UD and FG-V) of the fraction of volume of CNTs (Fig.1).

The volume fractions (Vcnt) of CNTs in two types of functionally graded carbon nanotube plates are stated as:

$$\left.\begin{aligned} V_{cnt}\ (Type-1) &= V_{cnt}^{*}\ (UD-CNT) \\ V_{cnt}\ (Type-2) &= \left(1-\frac{2z}{h}\right)V_{cnt}^{*}\ (FG-V\ \ CNT) \end{aligned}\right\} \quad (1)$$

$$V_{cnt}^{*} = \frac{w_{cnt}}{w_{cnt}+\frac{\rho_{cnt}}{\rho_m}-\left(\frac{\rho_{cnt}}{\rho_m}\right)w_{cnt}} \quad (2)$$

where, w_{cnt} represents the CNT mass fraction and ρ_{cnt} and ρ_m represent the densities of carbon nanotube and matrix, respectively. The material properties can be determined for this linear material property fluctuation by putting the value V_{cnt}^{*} into Eq. (1) for linear material property variation.

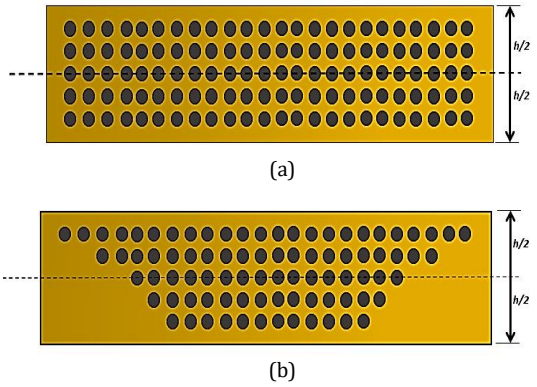

Fig. 1. (a) Uniformly distributed CNT nanocomposite plate, (b) V-Shape distributed CNT nanocomposite plate.

2.2. Modeling of Nanocomposite Material:

For predicting the properties of the material of CNT-reinforced composites, several micromechanical models have been proposed. In this research, the Mori–Tanaka technique is used to estimate the elastic properties of the equivalent fiber/polymer material. The equivalent inclusion average stress technique, commonly known as the Eshelby–Mori–Tanaka method, is based on Eshelby's [8] equivalent elastic inclusion notion and Mori-Tanaka's [6] concept of average stress inside the matrix. Benveniste's [9] revision of the effective modulus of elasticity tensor C of CNT-reinforced composites is as follows:

$$C = V_{cnt}\left\langle (C_r - C_m)A\right\rangle\left(V_m I + V_{cnt}\left\langle A_r\right\rangle\right)^{-1} + C_m \quad (3)$$

The symbol I is denoted as a fourth-order unit tensor. The matrix stiffness tensors are C_m, while the equivalent fiber stiffness tensors are C_r (CNT). The angle brackets in their overall configuration represent an average of all conceivable orientations for the inclusions A_r is the tensor of the concentration of dilute mechanical strain, and it can be calculated as follows:

$$A_r = \left[I + S\left(C_r - C_m\right)\left(C_m\right)^{-1} \right]^{-1} \tag{4}$$

Here symbol S represents the Eshelby tensor of the fourth order, as defined by Mura and Eshelby [8,10].

Here, a single-walled carbon nanotube having a solid cylinder of 1.424 nm diameter with (10,10) chirality index [11] is used for the analysis.

2.2.1. Randomly Oriented CNT-Reinforced Composites:

Straight carbon nanotube orientation is shown by two Euler angles α and β, denoted by the arrows in Fig. 2. As a result, the base vectors $\vec{e}_i$ of the global $(0-x_1\,x_2\,x_3)$ coordinate system and the base vectors $\vec{e}_i'$ of $(0-x_1'\,x_2'\,x_3')$ the local coordinate system are produced, which are related through the transformation matrix g, as follows:

$$\vec{e}_i = g\vec{e}_i^{\,r} \tag{5}$$

where g is given as:

$$g = \begin{bmatrix} \cos\beta & -\sin\beta\cos\alpha & \sin\beta\sin\alpha \\ \sin\beta & \cos\beta\cos\beta & -\cos\beta\sin\alpha \\ 0 & \sin\alpha & \cos\alpha \end{bmatrix} \tag{6}$$

It is possible to characterize the orientation distribution of carbon nanotubes in composites by the function of probability density p (α, β) that meets the normalizing condition.

$$\int_0^{2\pi}\int_0^{\pi/2} p(\alpha,\beta)\sin\alpha\, d\alpha\, d\beta = 1 \tag{7}$$

Considering the random CNT orientation, the function of density for this case is,

$$p(\alpha,\beta) = \frac{1}{2\pi} \tag{8}$$

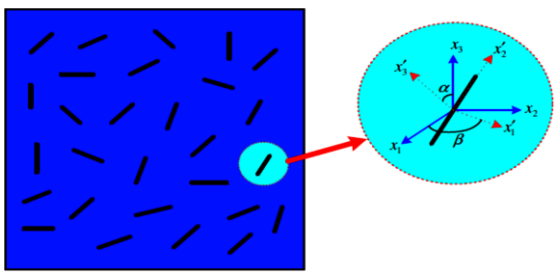

Fig. 2. Representative volume element (RVE) Composed of Randomly oriented, straight [12]

Calculation of Hill's elastic moduli for the reinforcing phase was accomplished by analyzing the equivalence of the two matrices that are presented below.[13]:

$$C_r = \begin{bmatrix} n_r & l_r & l_r & 0 & 0 & 0 \\ l_r & k_r + m_r & k_r - m_r & 0 & 0 & 0 \\ l_r & k_r - m_r & k_r + m_r & 0 & 0 & 0 \\ 0 & 0 & 0 & p_r & 0 & 0 \\ 0 & 0 & 0 & 0 & m_r & 0 \\ 0 & 0 & 0 & 0 & 0 & p_r \end{bmatrix}$$

$$= \begin{bmatrix} \frac{1}{E_L} & \frac{-\nu_{TL}}{E_T} & \frac{-\nu_{ZL}}{E_Z} & 0 & 0 & 0 \\ \frac{-\nu_{LT}}{E_L} & \frac{1}{E_T} & \frac{-\nu_{ZT}}{E_Z} & 0 & 0 & 0 \\ \frac{-\nu_{LZ}}{E_L} & \frac{-\nu_{TZ}}{E_T} & \frac{1}{E_Z} & 0 & 0 & 0 \\ 0 & 0 & 0 & \frac{1}{G_{TZ}} & 0 & 0 \\ 0 & 0 & 0 & 0 & \frac{1}{G_{TZ}} & 0 \\ 0 & 0 & 0 & 0 & 0 & \frac{1}{G_{LT}} \end{bmatrix}^{-1} \tag{9}$$

the terms k_r, l_r, m_r, n_r, and p_r in Eq. (9) represent Hill's elastic moduli for the reinforcing phase (CNTs) of the composite calculated by the inverse of the compliance matrix of the equivalent fiber. The values used for Hill's elastic moduli in this study are given in Table 1 [16].

As for the composite's properties E_L, E_T, E_Z, G_{LT}, G_{TZ}, G_{TZ}, and ν_{LT}, which may be established using the rule of mixture technique, the first step is to determine the properties of the composite by performing a multiscale finite element analysis or molecular dynamics simulation analysis [14] on the composite.

Here, the composite is considered isotropic when the carbon nanotubes are orientated randomly in nature in the matrix. For this the bulk modulus K and shear modulus G are calculated as follows:

$$K_{NC} = \frac{V_{cnt}\left(\delta_r - 3K_m\alpha_r\right)}{3\left(V_m + V_{cnt}\alpha_r\right)} + K_m \tag{10}$$

$$G_{NC} = \frac{V_{cnt}\left(\eta_r - 2G_m\beta_r\right)}{2\left(V_m + V_{cnt}\beta_r\right)} + G_m \tag{11}$$

The term K_m and G_m are used for bulk and shear moduli of the matrix respectively.

$$\alpha_r = \frac{3\left(K_m + G_m\right) + k_r - I_r}{3\left(G_m + k_r\right)} \tag{12}$$

$$\beta_r = \frac{1}{5}\left[\frac{4G_m + 2k_r + I_r}{3\left(G_m + k_r\right)} + \frac{4G_m}{G_m + p_r} + \frac{2\left[G_m\left(3K_m + G_m\right) + G_m\left(3K_m + 7G_m\right)\right]}{G_m\left(3K_m + G_m\right) + m_r\left(3K_m + 7G_m\right)} \right] \tag{13}$$

$$\delta_r = \frac{1}{3}\left[n_r + 2I_r + \frac{(2k_r + n_r)(3k_m + 2G_m - I_r)}{G_m + k_r} \right] \quad (14)$$

$$\eta_r = \frac{1}{5}\left[\begin{array}{l} \frac{2}{3}(n_r - I_r) + \frac{8G_m p_r}{G_m + p_r} + \\ \frac{(3K_m + 4G_m)8m_r G_m}{G_m(7m_r + G_m) + 3K_m(m_r + G_m)} + \\ \frac{2(I_r + 2G_m)(k_r - I_r)}{3(k_r + G_m)} \end{array} \right] \quad (15)$$

Finally, the modulus of elasticity and Poison ratio of a CNT-based nanocomposite material are as follows:

$$E_{NC} = \frac{9KG}{G + 3K} \quad (16)$$

$$v = \frac{3K - 2G}{2(G + 3K)} \quad (17)$$

Additionally, V_{cnt} and V_m represent the volume fractions of the carbon nanotubes and matrix, respectively, which fulfill the expression $V_{cnt} + V_m = 1$. Similarly, the mass density ρ is determined as follows:

$$\rho = \rho_{cnt} V_{cnt} + \rho_m V_m \quad (18)$$

where ρ_m and ρ_{cnt} represents the mass density of matrix and carbon nanotubes, respectively.

2.2.2. Agglomeration of Carbon Nanotubes

A large proportion of carbon nanotubes in carbon nanotube-reinforced composites has been found to be concentrated in agglomerates. Nanotubes agglomerate into bundles due to van der Waals's attractive interactions between them. After determining the material properties of FG-CNTRC without taking into account the CNT agglomeration effect, a new micromechanics model is developed and applied to a random-oriented, agglomerated CNT-reinforced polymer composite to determine the effective properties of the material of a single-walled CNT reinforced polymer composite while taking into account the CNTs bundling effect. The influence of agglomeration on the elastic characteristics of CNT-reinforced composites having random orientation is investigated in the present study, which uses a two-parameter micromechanics agglomeration model to do this.

As per Fig. 3, it can be seen that the elastic characteristics of the surrounding material are distinct from the areas where inclusions have concentrated nanotubes.

2.2.2.1. *Two Parameter Agglomeration Mode*l

In polymer matrix, the major cause of agglomeration of carbon nanotubes is a small diameter, due to which the elastic modulus gets reduced and the aspect ratio increases in the radial direction and hence produces low bending strength. Carbon nanotubes must be dispersed uniformly inside the matrix to achieve the desired features of CNT-reinforced composites. Here, a micromechanical model has been built to check the CNTs agglomeration effect on the effectiveness of carbon nanotube-enhanced elastic modules.

Shi et. al. [5] found that a substantial number of CNTs are concentrated in aggregates in the 7.5 % concentration sample. Carbon nanotubes are found to be unevenly distributed in the substrate, with a few areas having CNT concentrations larger than the average volume fraction. As illustrated in Fig. 3, these areas containing concentrated carbon nanotubes are considered spherical in this section and are referred to as 'inclusions' having a mix of varying elasticity characteristics from the surrounding material.

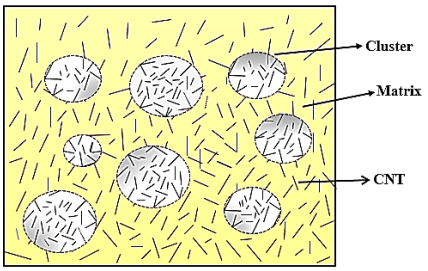

Fig. 3. Agglomeration of carbon nanotubes (CNTs) within the representative volume element (RVE)

The total volume V_r of CNTs in the RVE may be separated into two parts:

$$V_r = V_r^{inclusion} + V_r^{m} \quad (19)$$

where V_r^{m} and $V_r^{inclusion}$ are represented as the CNTs volume dispersed in the matrix and the inclusions (concentrated regions).

To understand clearly the effect of carbon nanotube agglomeration, two parameters are introduced as ξ and ζ.

$$\xi = \frac{V^{inclusion}}{V}, \zeta = \frac{V_r^{inclusion}}{V_r} \quad (20)$$

where $V_r^{inclusion}$ represents the volume of the RVE's sphere inclusions. In this case, ξ represents the volume of the inclusion fraction related to the RVE's total volume V. Whenever ξ is equal to one, CNTs are assumed to be distributed uniformly in the matrix, and as the value of ξ decreases, the degree of agglomeration of carbon nanotubes becomes more severe (Fig. 5 & Fig. 6). The symbol ζ denotes the nanotubes volume ratio distributed in the inclusions to the total volume of the CNTs. When the value ζ is 1,

all of the nanotubes are concentrated in the sphere regions. This is true if all nanotubes are dispersed evenly (i.e., $\zeta = \xi$) throughout the matrix (Fig. 4). As the value ζ increases (i.e., $\zeta > \xi$), the CNT's spatial distribution becomes more. The average carbon nanotube volume fraction in the composite is denoted by V_{cnt}.

$$V_{cnt} = \frac{V_r}{V} \tag{21}$$

The carbon nanotube's volume fractions in the inclusions and the matrix are calculated using Eqs. (19)-(21), and they are expressed as

$$\frac{V_r^{\ inclision}}{V^{\ inclusion}} = V_{cnt}\frac{\zeta}{\xi} \tag{22}$$

$$\frac{V_r^{\ m}}{V - V^{\ inclusion}} = \frac{V_{cnt}(1-\zeta)}{1-\xi} \tag{23}$$

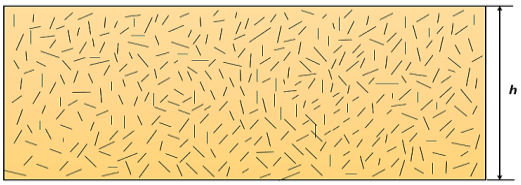

Fig. 4. $\varsigma = \xi = 1$ (Without agglomeration)

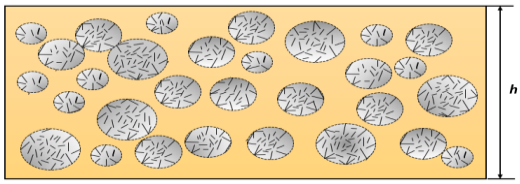

Fig. 5. $\varsigma = 1, \xi < \varsigma$ (Complete agglomeration)

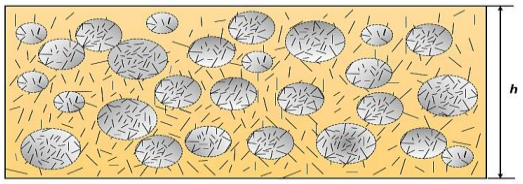

Fig. 6. $\varsigma < \xi, \xi < \varsigma$ (Partial agglomeration)

As a result, the Composite reinforced with carbon nanotubes is viewed as a system made up of sphere-shaped inclusions embedded in a hybrid matrix. CNTs can be found in both the matrix as well as in the inclusions also. Hence to compute the composite system's overall property first we have to estimate the inclusion's effective elastic stiffness and then the matrix.

Different micromechanics methods can be used to calculate the effective modulus of elasticity of the hybrid inclusions and matrix. Assuming that all CNT orientations are completely random and the nanotubes are transversely isotropic, the Mori-Tanaka scheme is used to estimate the hybrid matrix's elastic moduli, as described in the previous section. The carbon nanotubes are assumed to be oriented randomly within the inclusions, and thus the inclusions are isotropic. The term K_{in} and K_{out} represent the effective bulk moduli and G_{in} and G_{out} represent the effective shear moduli of the inclusions and matrix, respectively given as:

$$K_{in} = K_m + \frac{V_{cnt}\zeta(\delta_r - 3K_m\alpha_r)}{3(\xi - V_{cnt}\zeta + V_{cnt}\zeta\alpha_r)} \tag{24}$$

$$K_{out} = K_m + \frac{V_{cnt}(1-\zeta)(\delta_r - 3K_m\alpha_r)}{[3(1-\xi - V_{cnt}(1-\zeta) + V_{cnt}(1-\zeta)\alpha_r)]} \tag{25}$$

$$G_{in} = G_m + \frac{V_{cnt}\zeta(\eta_r - 2G_m\beta_r)}{2(\xi - V_{cnt}\zeta + V_{cnt}\zeta\beta_r)} \tag{26}$$

$$G_{out} = G_m + \frac{V_{cnt}(\eta_r - 2G_m\beta_r)(1-\zeta)}{[2(1-\xi - V_{cnt}(1-\zeta) + V_{cnt}\beta_r(1-\zeta))]} \tag{27}$$

Following that, the composite's effective bulk modulus *K* and effective shear modulus *G* are computed using the method of Mori-Tanaka as follows:

$$K = K_{out}\left[1 + \frac{\xi\left(\frac{K_{in}}{K_{out}} - 1\right)}{1 + \alpha(1-\xi)\left(\frac{K_{in}}{K_{out}} - 1\right)}\right] \tag{28}$$

$$G = G_{out}\left[1 + \frac{\xi\left(\frac{G_{in}}{G_{out}} - 1\right)}{1 + \beta(1-\xi)\left(\frac{G_{in}}{G_{out}} - 1\right)}\right] \tag{29}$$

where

$$\nu_{out} = \left(\frac{3K_{out} - 2G_{out}}{2(3K_{out} + G_{out})}\right),$$
$$\alpha = \frac{(1+\nu_{out})}{3(1-\nu_{out})}, \beta = \frac{(8-10\nu_{out})}{(15-15\nu_{out})} \tag{30}$$

Finally, the CNT-reinforced composite's young modulus is calculated using Eq. (16).

The mathematical formulations used in the next section are based on the following assumptions:

a. The midplane of the plate is taken as the reference plane.
b. The thickness of the plate is constant.
c. The kinematics field may have a cubic variation of thickness term in the in-plane part and a constant variation of thickness in the transverse displacement.
d. The interfaces are considered perfect.

3. Formulation

3.1. In-Plane Displacement Fields and Strains

The FGM plate's geometry used in this analysis is shown in Fig. 7. The plate's length and width are denoted by *a* and *b*, respectively, and its thickness is represented by *h*. The center of the FGCNT plate serves as the origin for material coordinates (*x*, *y*, and *z*). Plates are simply supported along their four edges, for the square plate. The aspect ratio considered is h/a = 0.1.

The in-plane displacement variation of *u*, *v*, and displacement in transverse direction *w* across the plate thickness may be described as using Reddy's theory of higher-order shear deformation [15].

$$\begin{aligned} u(x,y,z) &= u_0 + z\,\theta_x - \frac{4z^3}{3h^2}\gamma_x \\ v(x,y,z) &= v_0 + z\,\theta_y - \frac{4z^3}{3h^2}\gamma_y \\ w(x,y) &= w_0 \end{aligned} \tag{31}$$

where u_0, v_0 and w_0 signify the displacement of a point along the (x, y, z) coordinates located at mid-plane, respectively, θ_x and θ_y denotes the bending rotations in the y and x directions, respectively, and γ_x & γ_y denotes the shear rotations assumed in the x, y directions.

The relationship between the strain component and the strain displacement is defined as follows:

$$\{\varepsilon_m\} = \begin{Bmatrix} \frac{\partial u}{\partial x} \\ \frac{\partial v}{\partial y} \\ \frac{\partial u}{\partial y} + \frac{\partial v}{\partial x} \\ \frac{\partial u}{\partial z} + \frac{\partial w}{\partial x} \\ \frac{\partial v}{\partial z} + \frac{\partial w}{\partial y} \end{Bmatrix} = \begin{Bmatrix} \frac{\partial u_0}{\partial x} + z\frac{\partial \theta_x}{\partial x} - \frac{4z^3}{3h^2}\frac{\partial \gamma_x}{\partial x} \\ \frac{\partial v_0}{\partial y} + z\frac{\partial \theta_y}{\partial y} - \frac{4z^3}{3h^2}\frac{\partial \gamma_x}{\partial y} \\ \frac{\partial u_0}{\partial y} + z\frac{\partial \theta_x}{\partial x} - \frac{4z^3}{3h^2}\frac{\partial \gamma_x}{\partial x} + \frac{\partial v_0}{\partial y} + z\frac{\partial \theta_y}{\partial y} - \frac{4z^3}{3h^2}\frac{\partial \gamma_x}{\partial y} \\ \frac{\partial w_0}{\partial x} + \theta_x - \frac{4z^3}{h^2}\gamma_x \\ \frac{\partial w_0}{\partial y} + \theta_y - \frac{4z^2}{h^2}\gamma_y \end{Bmatrix} \tag{32}$$

The overall strain may be represented as mechanical strains for plate analysis.

$$\{\varepsilon\} = \{\varepsilon_m\} \tag{33}$$

where ε_m represents the mechanical strain.

Again, in terms of total strain, the mechanical strain may be represented as

$$\{\varepsilon_m\} = [H]\{\varepsilon\} \tag{34}$$

while $[H]$ is the thickness coordinates-z function, and $\{\varepsilon\}$ is the function of x and y.

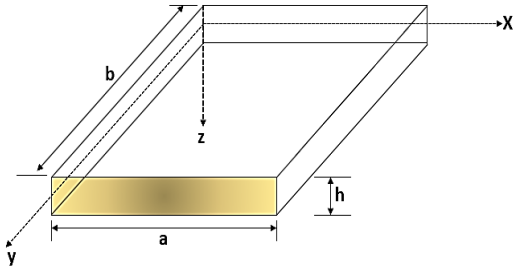

Fig. 7. Geometry of the FGCNT Plate

This describes the overall strain as,

$$\{\varepsilon\} = [H]\{\varepsilon\} \tag{35}$$

3.2. Constitutive Relationship

The relation between stress and strain for FGM is as follows:

$$\{\sigma\} = [Q]\{\varepsilon\} \tag{36}$$

where constitutive matrix

$$[Q] = \begin{bmatrix} Q_{11} & Q_{12} & 0 & 0 & 0 \\ Q_{21} & Q_{22} & 0 & 0 & 0 \\ 0 & 0 & Q_{33} & 0 & 0 \\ 0 & 0 & 0 & Q_{44} & 0 \\ 0 & 0 & 0 & 0 & Q_{55} \end{bmatrix} \tag{37}$$

In Eq. (37) the term Q_{ij} is derived from the FG material properties, depending on the plate's thickness (z) as shown below in Eq. (38).

$$\begin{aligned} Q_{11} &= Q_{22} = \frac{E}{1-\gamma^2} \\ Q_{12} &= Q_{21} = \frac{\gamma E}{1-\gamma^2} \\ Q_{33} &= Q_{44} = Q_{55} = \frac{E}{2(1+\gamma)} \end{aligned} \tag{38}$$

3.3. Virtual Work in FGCNT Plate

The FGM plate's virtual work may be represented as

$$\delta U = \iiint \{\delta\varepsilon\}^T \{\sigma\}\, dx\, dy\, dz \tag{39}$$

With the help of Eq. (36), Eq. (39) can be rewritten as

$$\delta U = \iiint \{\delta\varepsilon\}^T [Q]\{\varepsilon\}\, dx dy dz \tag{40}$$

The following equation can be extended further using Eq. (35) as follows:

$$\delta U = \iiint \{\delta\varepsilon\}^T [H]^T [Q][H]\{\varepsilon\}\, dx dy dz \tag{41}$$

In Eq. (41) the matrix [Q] represents the constitutive matrix with elasticity derived from the constituent's elastic properties as given in Eq. (37). While *[H]* represents the 5 x 15 order matrix and includes the terms *z* and *h* as described below:

$$[H]=\begin{bmatrix} 1&0&0&0&0&z&0&0&0&0&0&0&\frac{-4z^3}{3h^2}&0&0\\ 0&1&0&0&0&0&z&0&0&0&0&0&0&\frac{-4z^3}{3h^2}&0\\ 0&0&1&0&0&0&0&z&0&0&0&0&0&0&\frac{-4z^3}{3h^2}\\ 0&0&0&1&0&0&0&0&1&0&\frac{-4z^2}{h^2}&0&0&0&0\\ 0&0&0&0&1&0&0&0&0&1&0&\frac{-4z^2}{h^2}&0&0&0 \end{bmatrix} \quad (42)$$

Finally, we can rewrite Eq. (41) as:

$$\delta U = \iint \{\delta\varepsilon\}^T [D]\{\varepsilon\}\, dxdy \quad (43)$$

where matrix represents the rigidity matrix vector. For which the corresponding expression is given in Eq. (44) shown below.

$$[D] = \int_{\frac{-h}{2}}^{\frac{h}{2}} [H]^T [Q][H] dz \quad (44)$$

4. Finite Element Formulation

4.1. Element Description

Fig. 8 illustrates the isoparametric Lagrangian element's geometry with nine nodes used in the analysis. In this element, there is a total of sixty-three degrees of freedom (DoF) because each node has seven degrees of freedom (*u, v, w,* θ_x , θ_y , γ_x and γ_y). In the x-y plane coordinate system, this element has a rectangular geometry that is completely arbitrary. The element is transferred to $\xi-\eta$ plane in order to get a rectangular geometry.

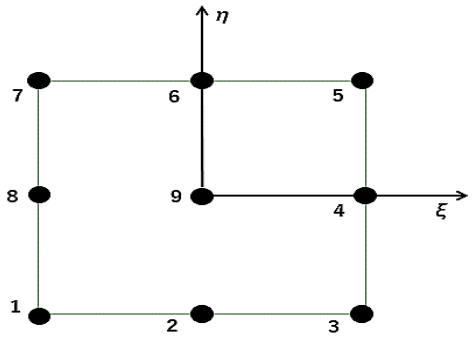

Fig. 8. Nine Node Iso-parametric Element with node numbering

The relationship between strain and displacement can be established using the nine shape functions as per node numbering given in Fig. 8. The vector of a strain can be expressed in the following way:

$$\{\varepsilon\} = [B]\{X\} \quad (45)$$

In Eq. (45) matrix [B] represents the strain-displacement matrix and matrix [X] represents the vector of nodal displacement for the element chosen and both matrices can be represented as follows:

$$[B] = [B_1 \;\; B_2 \;\; B_3 \;\; B_4 \;\; B_5 \;\; B_6 \;\; B_7 \;\; B_8 \;\; B_9],$$
$$\{X\} = [X_1 \;\; X_2 \;\; X_3 \;\; X_4 \;\; X_5 \;\; X_6 \;\; X_7 \;\; X_8 \;\; X_9] \quad (46)$$

4.2. Governing Equations used for Static Analysis

For the bending analysis of the FGCNT plate, the following equation is used to obtain the governing equation. The variation of the strain vector can be expressed as follows using Eq. (46).

$$\{\delta\varepsilon\} = [B]\{\delta X\} \quad (47)$$

By combining Eqs. (43) & (47), the following expression can be obtained.

$$\delta U = \{\delta X\}^T \left[\left(\iint [B]^T [D][B] dx\, dy\right)\{X\}\right] \quad (48)$$

The vector of stiffness can be represented in the following manner using Eq (49).

$$[K] = \iint [B]^T [D][B] dx\, dy \quad (49)$$

5. Numerical results & discussion

In this section, the static analysis of the FG plate with different distributions of carbon nanotube (Fig. 1) has been done by considering various agglomeration states as shown in Fig. (4)–(6). This section is separated into two distinct sections. The first phase involves a convergence study and validation of the current formulation for isotropic plates with varying aspect ratios, as no solution exists for the current problem. The conclusion is reported solely for the situation of uniformly distributed load. After confirming the effectiveness of the current formulation, the second step investigates the impacts of various agglomeration states on the central deflections and axial stresses of the FG plate.

Table 1. Hill's elastic moduli for several Single-Walled Carbon Nanotubes (SWCNT) [16].

Carbon nanotubes	k_r[GPa]	l_r[GPa]	m_r[GPa]	n_r[GPa]	p_r[GPa]
SWCNT (10,10)	271	88	17	1089	442

5.1. Isotropic Plate Subjected to UDL Load Of Intensity q: Convergence and Validation Study:

The dimension of the isotropic plate for analysis is taken as a = b. The coordinate system's origins (x, y, and z) are set to the plate's mid-plane (i.e., z = 0). For isotropic plates having E = 10.92 x 10^6 N/m^2 and υ = 0.3 the Convergence study and validation study for displacement-associated parameters are carried out as shown in Table 2. Several values of aspect ratio h/a = 0.1, 0.01 are considered with simply supported boundary conditions. According to the results of the convergence investigation, a 16 x 16 mesh is sufficient for flexural analysis when using the current isoparametric Lagrangian element with nine nodes. As a result, for all subsequent examples involving agglomerated functionally graded plates, a 16 x 16 mesh is used. The non-dimensional parameters for deflection at the center point, vertically applied load, and considered thickness coordinates (z) are: $\bar{w} = w/h, q_o = q/E_m h^4$, $\bar{z} = z/h$. The results are compared with those represented by Sheikh et. al. which are based on a new plate-bending element based on higher-order theory, studied in the framework of the finite element method. For a thin plate ratio of h/a = 0.01, the present results are compared and very close agreements are noted between the results obtained from the two approaches.

For the displacement field given in Eq. (31), the following types of boundary conditions are used in the analysis.

Simply supported (SSSS):

$v = w = \theta_y = \gamma_y = 0$ at x = 0, a

$u = w = \theta_x = \gamma_x = 0$ at y = 0, b

Clamped (CCCC):

$u = v = w = \theta_x = \theta_y = \gamma_y = \gamma_x = 0$ at x = 0, a and y = 0, b.

Table 2. Central Deflection $100wD/qa^4$ square plate (SSSS) under the applied uniform load of intensity qo = 0.1 MPa.

No. of Element	Ref. [7] (h/a =0.01)	Present (h/a=0.01)
2 x 2	0.4264	0.1669
3 x 3	0.4095	0.1297
4 x 4	0.4089	0.2094
6 x 6	0.4074	0.3355
8 x 8	0.4071	0.3805
12 x 12	0.4067	0.4009
16 x 16	0.4066	0.4046

After verification of the present model, the main aim of this study was to see the effect of agglomeration with various CNT distributions (Fig. 1) on a deflection at the center point of a simply supported square plate. These are presented in the next section.

5.2. Flexural Behavior of CNT Reinforced Functionally Graded Simply Supported Square Plate with Three Different Stages of Agglomeration:

In the following subsections, the flexural behavior of the square plate (Fig. 7) is evaluated using nine noded isoparametric Lagrangian elements with 16 x 16 mesh division, and further results are discussed in detail in Sections 5.2.1, 5.2.2 & 5.2.3 with various agglomeration schemes namely, (i). square plate without agglomeration effect $(\varsigma = \xi = 1)$, (ii). Square plate with complete agglomeration effect $(\varsigma = 1, \xi < \varsigma)$, (iii) square plate with partial agglomeration effect $(\varsigma < \xi, \xi < \varsigma)$. The matrix material used in the study possesses the following elastic properties: E_m=2.1 GPa, υ_m=0.34, and the properties of SWCNT (10,10) are listed in Table 1. A value of V_{cnt}^* is considered with a concentration value of 7.5 %, which indicates the presence of a large number of CNTs [2]. In all the above states, the influence of different boundary conditions (SSSS and CCCC) with two different CNT distribution (UD & FG-V) patterns is considered for the analysis.

5.2.1. Square Plate Without the Agglomeration Effect:

This study does not consider an agglomerated state, as ζ = ξ and its results serve as a reference for the next two agglomeration states as given in Sections 5.2.2 & 5.2.3. It is understood that when compared to the other two distributions, the FG-V provides the best flexural behavior since its deflection assumes lesser values. This behavior is attained because the CNTs are in higher concentrations distributed to higher stress regions.

Figure 9 shows the axial stress distribution across the plate thickness for the UD and FG-V distribution of CNTs without the agglomeration effect, noting that stresses are well distributed in the case of UD and FG-V distribution. One can see the stress distribution pattern in the case of UD follows a similar value of tensile and compressive stress above and below the midplane. While in the case of FG-V distribution there is gradual stress drop occurs because of CNT'ss fraction decrement below the midplane forming a V-type distribution pattern.

From Table 3 one can observe that the deflection values for no agglomeration case show intermediate behavior as compared to the other two states of agglomeration. From all the above parametric studies we can conclude that better flexural behavior is observed in case of no agglomeration as compared to complete and partial stages of agglomeration.

Table. 3 Non-dimensional Central Deflection (w/h) for aspect ratio (h/a = 0.1) & $V_{cnt}^{*}=0.075$

Agglomeration Stage		UD	FG-V	UD	FG-V
		SSSS		CCCC	
Without agglomeration	ζ=0.25, ξ=0.25	0.0120	0.0128	0.00463	0.0045

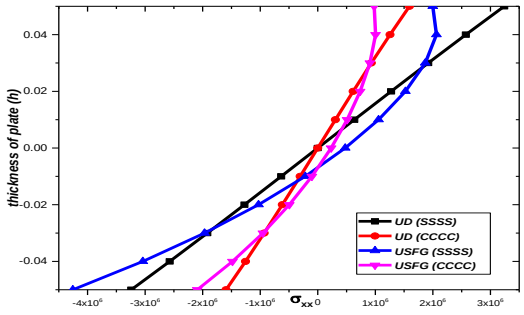

Fig. 9. Variation of axial stress (σ_{xx}) through-the-thickness for square plate subjected to a normal pressure qo = -0.1 MPa on the top surface without agglomeration case. ζ= 0.25 & ξ= 0.25.

5.2.2. Square Plate with Complete Agglomeration Effect:

This study comprehends a complete state of agglomeration, when ζ = 1 for three different values of ξ = [0.15, 0.45, 0.75] (i.e., complete agglomeration). It is assumed that in these agglomerated states, all CNTs are bundled into spherically shaped inclusions.

From the three cases of complete agglomerations considered here, it may be observed that the worst flexural behavior occurs when ξ = 0.15, the CNT distribution is most diverse and aggregation is most severe. These three developed cases under a complete agglomeration state reveal that the bigger the difference between the values of agglomeration parameters, the more its elastic properties would be affected by the agglomeration of CNTs.

In Table 4 it can be seen as ξ increases, the deflection values of UD and FG-V distributed CNT reinforced composite plate decrease. For the complete agglomeration case, the stiffness of the FG-V type distribution is less as compared to the UD distribution. Simultaneously the variation of non-dimensional axial stress (σ_{xx}) at the plate center for two boundary conditions (SSSS and CCCC) and aspect ratio (h/a) 0.1 and 0.01 is also plotted as shown in Fig. 12 to clearly understand the behavior of UD and FG-V distributed CNT including nanocomposite plate for V_{cnt}^{*} = 0.075. From the stress diagram, it could be understood that stress variation across the thickness in the third case of the complete agglomeration state shows similar behavior to the other two states of agglomeration.

The results presented in Table 4 itself show that for all cases of complete agglomerations, the FG-V CNT distribution has the worst flexural behavior when compared with the same state of agglomeration for UD distribution. Here to visualize the complete agglomeration behaviour one can see, for other higher values of parameter ζ, when the parameter ξ is taken as 0.15 corresponding to ζ=1 (i.e., the most heterogeneous distribution of CNTs), shows a more severe level of agglomeration effect both for UD and FG-V type (Fig. 10 & 11).

Table. 4. Non-dimensional Central Deflection (w/h) for aspect ratio (h/a = 0.1) & $V_{cnt}^{*}=0.075$.

Agglomeration Stage		UD-CNTRC	FG-V CNTRC	UD-CNTRC	FG-V CNTRC
		SSSS		CCCC	
Complete Agglomeration	ζ = 1, ξ=0.15	0.01724	0.01788	0.00609	0.00631
	ζ =1, ξ=0.45	0.01436	0.01514	0.00511	0.00536
	ζ = 1, ξ=0.75	0.01290	0.01368	0.00464	0.00487

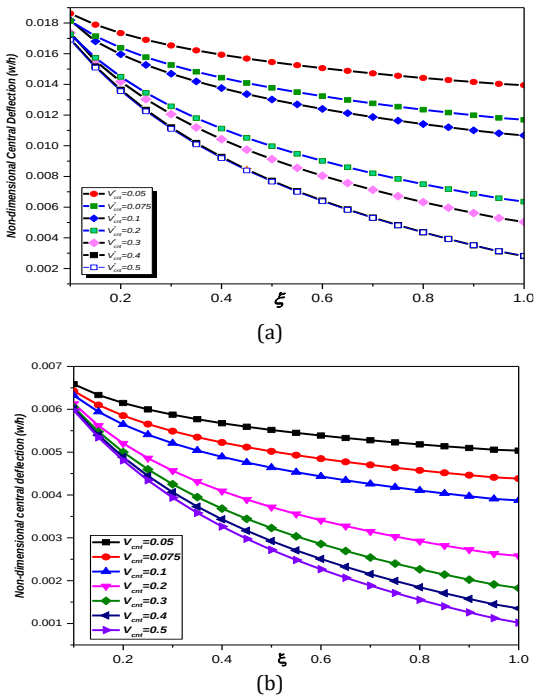

Fig. 10. Non-dimensional central deflection of plate vs ξ [(a) SSSS case, (b) CCCC Case] for Complete Agglomeration case ($\varsigma=1, \xi<\varsigma$) with UD distribution of CNT across the thickness direction of the plate.

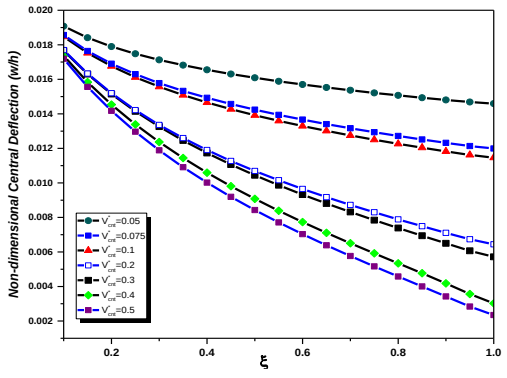

(a)

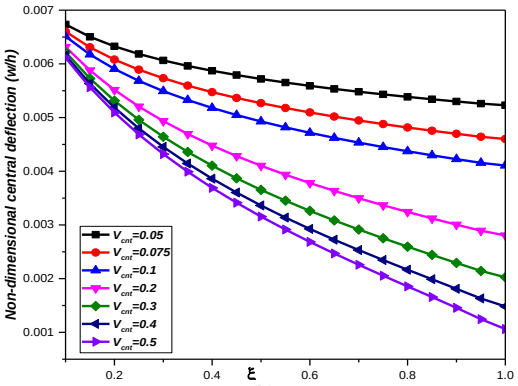

(b)

Fig. 11. Non-dimensional central deflection of plate vs ξ [(a) SSSS case, (b) CCCC Case] for Complete Agglomeration case ($\varsigma=1, \xi<\varsigma$) with unsymmetrical distribution of CNT (FG-V Type).

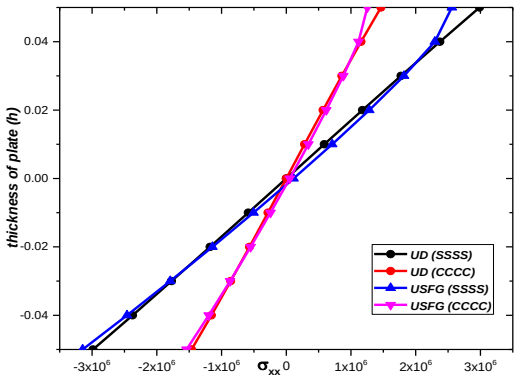

(a)

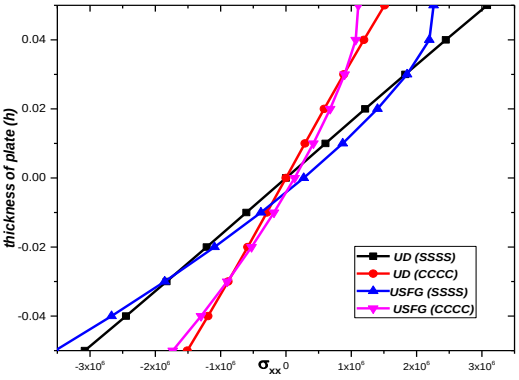

(b)

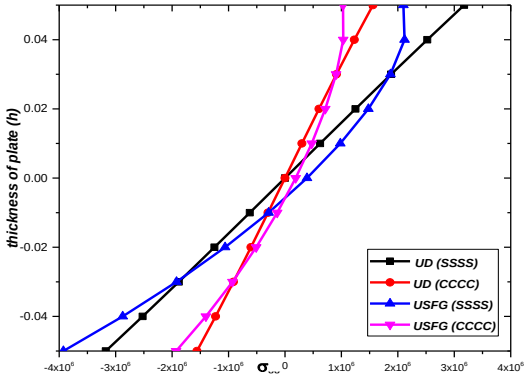

(c)

Fig. 12. Variation of axial stress (σ_{xx}) through the thickness of square plate subjected to UDL of intensity qo = -0.1 MPa on the top surface for complete agglomeration case. (a) ζ=1 & ξ= 0.15, (b) ζ=1 & ξ= 0.45, (c) ζ=1 & ξ= 0.75.

Globally, one can say that for a completely agglomerated case, the more heterogenous the distribution, the higher the deflection values will be as compared to the UD distribution studied. It is also possible to conclude that besides the level of agglomeration, the UD distribution shows a better flexural behavior due to its even distribution of CNTs even in higher bending stress areas.

5.2.3. Square Plate with Partial Agglomeration Effect:

In this study the third possibility assumes that this case is distinct from the no agglomerated state or completely agglomerated state, hence being very important to achieve a plausible description of the level of agglomeration through the parameters ζ and ξ. Here, to investigate the flexural behavior of square plate for two assumed CNT distribution patterns (UD & FG-V), two different partially agglomerated situations were developed and evaluated as given in Table 5.

Table. 5 Non-dimensional Central Deflection (w/h) for aspect ratio (h/a = 0.1) & $V^*_{cnt}=0.075$

Agglomeration Stage		UD-CNTRC	FG-V CNTRC	UD-CNTRC	FG-V CNTRC
		SSSS		CCCC	
Partial Agglomeration	ζ=0.25, ξ=0.4	0.0123	0.0129	0.0043	0.0046
	ζ=0.75, ξ=0.4	0.01235	0.01306	0.0045	0.0047

From Table 5, when comparing the two cases of partial agglomeration state, the best flexural behavior is achieved with ζ=0.25 and ξ=0.4, which corresponds to a case where there is less volume fraction of CNTs in agglomerated inclusions, as compared to the second case where ζ=0.75 and ξ=0.4.

It was also observed that deflection values remained unchanged despite the agglomeration effect compared to the results obtained for the no agglomeration state. Similarly, the conclusion can be drawn from the stress distribution diagram (Fig. 13) for this particular state that the stress distribution pattern and values are almost close to no agglomeration state for both types of CNT distributions (UD & FG-V).

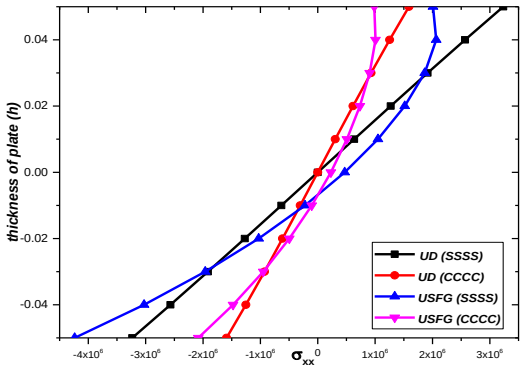

(a)

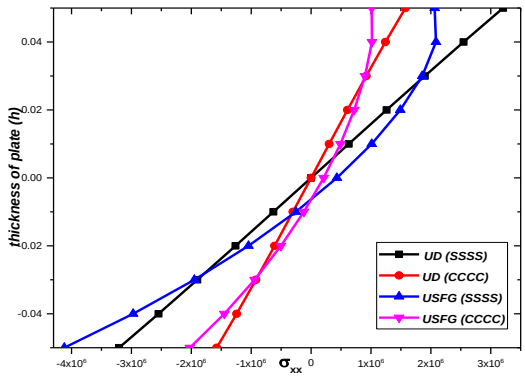

(b)

Fig. 13. Variation of axial stress (σ_{xx}) through-the-thickness for square plate subjected to a normal pressure qo = -0.1 MPa on the top surface for partial agglomeration case (a)ζ=0.25 & ξ= 0.4, (a)ζ=0.75 & ξ= 0.4.

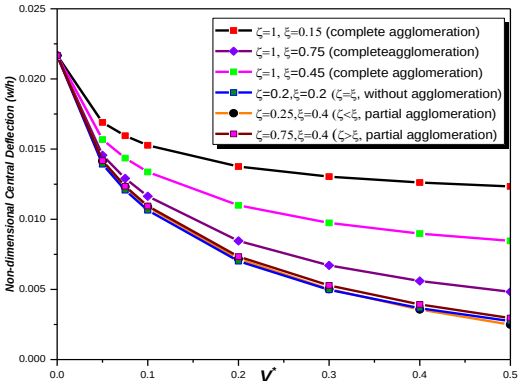

(a)

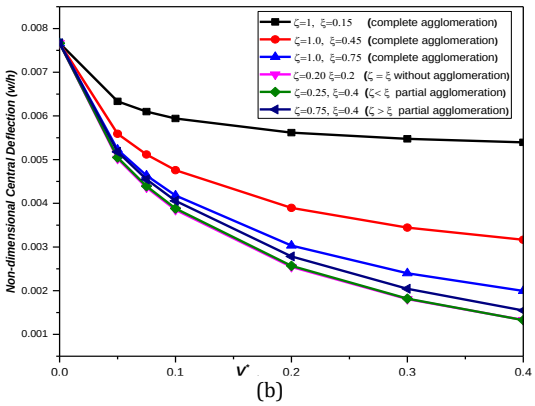

(b)

Fig. 14. Effect of agglomeration parameter (ς, ξ) on non-dimensional central deflection [(a) SSSS case, (b) CCCC Case] of uniformly distributed CNT reinforced square (a = b =1) nanocomposite plate.

From Fig. 14, it can be observed that agglomeration reduces the stiffness, which if not considered gives overestimated values. For this Fig. 14 is plotted between non-dimensional central deflection and various values of V_{cnt}^{*}.

6. Conclusions

Under mechanical loading, the behavior of FGCNT plates with an agglomeration effect is investigated using an efficient C^0 FE model using the theory of HSDT. It is possible to compute the effective material properties of agglomerated carbon nanotube reinforced plate by utilizing a two-parameter agglomeration model based on the Eshelby–Mori–Tanaka scheme for dispersed nano-inclusions oriented randomly in nature, which is again briefed from the Eshelby–Mori–Tanaka technique. The study's key findings are outlined below. Because carbon nanotubes tend to agglomerate at very little CNT volume fractions, an important conclusion can be drawn:

- Failing to account for the effect of CNT agglomeration may result in an overestimation of the elastic properties of CNT-reinforced nanocomposite, resulting in a less accurate prediction of structural behavior.
- The non-dimensional central deflection increases for a lesser value of ξ & ζ=1 in case of complete agglomeration.
- The non-dimensional central deflection without agglomeration (ζ= ξ) shows better flexural behavior as compared to the complete and partial state of agglomeration.

- The flexural behavior in the case of the partial agglomeration state is approximately close to that without the agglomeration state.
- The UD distribution shows better flexural behavior in all three stages of agglomeration as compared to FG-V type CNT distribution through the thickness.
- In the present study, a new model has been proposed that considered the effect of agglomeration in CNT-reinforced plates using the HOST theory. Finally, new results are generated which should be useful for future studies.

Nomenclature

CNT	Carbon nanotube
FG	Functionally Graded Materials
H	Thickness
UD	Uniformly Distributed
V_{cnt}^{*}	Carbon nanotube volume fraction
SSSS	All four edges simply supported
CCCC	All four edges clamped
FG-V	V-Type CNT distribution pattern along the thickness direction
ξ, ζ	Agglomeration parameter
N_i	Shape function

Acknowledgments

The authors would like to acknowledge Madan Mohan Malaviya University of Technology, Gorakhpur U.P-273010 India for the financial support of this work.

Conflicts of Interest

The corresponding author declares that there are no competing interests on behalf of the other authors.

References

[1] Radushkevich, L.V. and Lukyanovich, V.Á., 1952. O strukture ugleroda, obrazujucegosja pri termiceskom razlozenii okisi ugleroda na zeleznom kontakte. Zurn Fisic Chim, 26(1), pp.88-95.

[2] Stephan, C., Nguyen, T.P., De La Chapelle, M. L., Lefrant, S., Journet, C. and Bernier, P., 2000. Characterization of single-walled carbon nanotubes-PMMA composites. Synthetic Metals, 108(2), pp.139-149.

[3] Zhu, P., Lei, Z.X. and Liew, K.M., 2012. Static and free vibration analyses of carbon nanotube-reinforced composite plates using finite element method with first-order shear deformation plate theory. Composite Structures, 94(4), pp.1450-1460.

[4] 4hen, H.S., 2013. Thermal buckling and post-buckling of functionally graded fiber-reinforced composite laminated plates. Journal of composite materials, 47(22), pp.2783-2795.

[5] Shi, D.L., Feng, X.Q., Huang, Y.Y., Hwang, K.C. and Gao, H., 2004. The effect of nanotube waviness and agglomeration on the elastic property of carbon nanotube-reinforced composites. J. Eng. Mater. Technol., 126(3), pp.250-257.

[6] Mori, T. and Tanaka, K., 1973. Average stress in matrix and average elastic energy of materials with misfitting inclusions. Acta metallurgica, 21(5), pp.571-574.

[7] Tornabene, F., Fantuzzi, N. and Bacciocchi, M., 2017. Linear static response of nanocomposite plates and shells reinforced by agglomerated carbon nanotubes. Composites Part B: Engineering, 115, pp.449-476.

[8] Eshelby, J.D., 1957. The determination of the elastic field of an ellipsoidal inclusion, and related problems. Proceedings of the royal society of London. Series A. Mathematical and physical sciences, 241(1226), pp.376-396.

[9] Benveniste, Y., 1987. A new approach to the application of Mori-Tanaka's theory in composite materials. Mechanics of materials, 6(2), pp.147-157.

[10] Mura, T., 1987. Mechanics of elastic and inelastic solids. In Micromechanics of Defects in Solids. Martinus Nijhoff Publishers Dordrecht.

[11] Shokrieh, M.M. and Rafiee, R., 2010. On the tensile behavior of an embedded carbon nanotube in polymer matrix with non-bonded interphase region. Composite Structures, 92(3), pp.647-652.

[12] Aragh, B.S., Barati, A.N. and Hedayati, H., 2012. Eshelby–Mori–Tanaka approach for vibrational behavior of continuously graded carbon nanotube-reinforced cylindrical panels. Composites Part B: Engineering, 43(4), pp.1943-1954.

[13] Yas, M.H. and Heshmati, M., 2012. Dynamic analysis of functionally graded nanocomposite beams reinforced by randomly oriented carbon nanotube under the action of moving load. Applied Mathematical Modelling, 36(4), pp.1371-1394.

[14] Kamarian, S., Shakeri, M., Yas, M.H., Bodaghi, M. and Pourasghar, A., 2015. Free vibration analysis of functionally graded nanocomposite sandwich beams resting on

Pasternak foundation by considering the agglomeration effect of CNTs. Journal of Sandwich Structures & Materials, 17(6), pp.632-665.

[15] Taj, M.G., Chakrabarti, A. and Sheikh, A.H., 2013. Analysis of functionally graded plates using higher order shear deformation theory. Applied Mathematical Modelling, 37(18-19), pp.8484-8494.

[16] Shen, L. and Li, J., 2004. Transversely isotropic elastic properties of single-walled carbon nanotubes. Physical Review B, 69(4), p.045414.

[17] Ansari, M.I., Kumar, A., Barnat-Hunek, D., Suchorab, Z., Andrzejuk, W. and Majerek, D., 2018. Static and dynamic response of FG-CNT-reinforced rhombic laminates. Applied Sciences, 8(5), p.834.

[18] Ansari, M.I., Kumar, A., Fic, S. and Barnat-Hunek, D., 2018. Flexural and free vibration analysis of CNT-reinforced functionally graded plate. Materials, 11(12), p.2387.

[19] Ansari, M.I. and Kumar, A., 2019. Flexural analysis of functionally graded CNT-reinforced doubly curved singly ruled composite truncated cone. Journal of Aerospace Engineering, 32(2), p.04018154.

[20] Ansari, M.I. and Kumar, A., 2019. Bending analysis of functionally graded CNT reinforced doubly curved singly ruled truncated rhombic cone. Mechanics Based Design of Structures and Machines, 47(1), pp.67-86.

[21] Kumar, R. and Kumar, A., 2022. Free vibration response of cnt-reinforced multiscale functionally graded plates using the modified shear deformation theory. Advances in Materials and Processing Technologies, pp.1-23.

[22] Zghal, S., Frikha, A. and Dammak, F., 2017. Static analysis of functionally graded carbon nanotube-reinforced plate and shell structures. Composite Structures, 176, pp.1107-1123.

[23] Zghal, S., Frikha, A. and Dammak, F., 2018. Free vibration analysis of carbon nanotube-reinforced functionally graded composite shell structures. Applied Mathematical Modelling, 53, pp.132-155.

[24] Zghal, S., Frikha, A. and Dammak, F., 2018. Mechanical buckling analysis of functionally graded power-based and carbon nanotubes-reinforced composite plates and curved panels. Composites Part B: Engineering, 150, pp.165-183.

[25] Frikha, A., Zghal, S. and Dammak, F., 2018. Dynamic analysis of functionally graded carbon nanotubes-reinforced plate and shell structures using a double directors finite shell element. Aerospace Science and Technology, 78, pp.438-451.

[26] Frikha, A., Zghal, S. and Dammak, F., 2018. Finite rotation three and four nodes shell elements for functionally graded carbon nanotubes-reinforced thin composite shells analysis. Computer Methods in Applied Mechanics and Engineering, 329, pp.289-311.

[27] Zghal, S., Frikha, A. and Dammak, F., 2018. Non-linear bending analysis of nanocomposites reinforced by graphene-nanotubes with finite shell element and membrane enhancement. Engineering structures, 158, pp.95-109.

[28] Zghal, S., Frikha, A. and Dammak, F., 2020. Large deflection response-based geometrical nonlinearity of nanocomposite structures reinforced with carbon nanotubes. Applied Mathematics and Mechanics, 41(8), pp.1227-1250.

[29] Odegard, G.M., Clancy, T.C. and Gates, T.S., 2017. Modeling of the mechanical properties of nanoparticle/polymer composites. In Characterization of Nanocomposites (pp. 319-342). Jenny Stanford Publishing.